A fluid cell with integrated acoustic radiation pressure actuator for atomic force microscopy

A. G. Onaran and F. L. Degertekin[a)]
G. W. Woodruff School of Mechanical Engineering, Georgia Institute of Technology, Atlanta, Georgia 30332-0405

The development of a fluid cell with an acoustic radiation pressure (ARP) actuator for atomic force microscopy (AFM) is reported. The ARP actuator uses a zinc oxide thin film transducer fabricated on a silicon substrate to generate acoustic waves in the 120–180 MHz range. These waves are coupled to the liquid and are reflected off of the AFM cantilever exerting radiation pressure to move the AFM cantilevers in the dc-MHz frequency range, providing a fast actuation scheme. Since the ARP actuator is remotely located on the fluid cell, it can be used with virtually any type of cantilever. The design, fabrication, and characterization of the AFM fluid cell with an ARP actuator are discussed and the performance of the device is compared with theoretical predictions. ARP actuator electronics and its integration to a commercial AFM system are described. Tapping mode images and molecular adhesion measurements are presented as illustrative examples. © *2005 American Institute of Physics.* [DOI: 10.1063/1.2069627]

I. INTRODUCTION

The importance and variety of atomic force microscopy (AFM) applications in liquids for imaging and measurement of biological samples and chemical processes has been increasing along with the demands on the AFM system performance. For imaging applications in liquids, the tapping mode is commonly used to minimize damage to the sample.[1,2] This mode of imaging requires an actuation scheme capable of exciting the cantilever resonances without any spurious resonances.[3] Since many biological and chemical processes occur in less than a minute, one needs fast, yet soft, cantilevers (high resonance frequency) and broadband actuators to drive them.[4] The AFM has also been used to perform force spectroscopy measurements on a variety of molecules to determine parameters such as bond life, intermolecular forces, and molecular structure.[5] In addition to the advantage of faster measurement times to shrink the separation between the time scales of force spectroscopy experiments, parallel measurements would be required to verify statistical models used for characterization biomolecular interactions.[6] An array of individually actuated cantilevers can speed up this process significantly, as in the case of parallel imaging applications.[7] Furthermore, quicker scan speeds will reduce the time spent locating interesting features and enable the study of dynamics occurring in liquid or physiological environments.[8]

Cantilever actuation schemes used in current AFM systems do not satisfy these demanding requirements simultaneously. Conventional AFM systems use a piezotube as the *z*-axis actuator for both dc and ac actuation. Therefore, the speed of the AFM is limited by the resonant frequency of the piezotube, which is typically in the several kHz range, corresponding to scan speeds of $10-50\ \mu m/s$. A direct approach to overcome these limitations uses smaller cantilevers with open loop operation or to reduce the size of the actuation hardware including the piezoelectric stack. This approach has been successfully used to view myosin V molecules moving around on mica with a frame rate of 12.5 frames/s, with a tip speed of 0.6 mm/s.[8] However, these approaches cannot be transferred directly to commercial AFM systems for wider use, and are not suitable for scaling up in the form of arrays.

Among many proposed actuation methods for fast imaging, one of the promising approaches so far involves integration of a thin film piezoelectric actuator onto the AFM cantilever.[9] With this structure, the cantilever is moved by the voltage applied to the zinc oxide (ZnO) transducer terminals, both for *z* positioning and for tapping operation. Furthermore, this actuator can be used to actively control the vibration characteristics of the cantilever.[10] However, there are some drawbacks of this actuator. The piezoelectric film electrodes should be passivated for immersion applications, which results in degradation of the tip sharpness.[11] More importantly, integration of the piezoelectric actuator puts limitations on the material, geometry and the stiffness of the cantilevers. The high stress in the ZnO films makes it difficult to build thin cantilevers with desired stiffness. It has not been possible, for example, to integrate piezoelectric actuators to soft cantilevers required for imaging biological samples and force spectroscopy of biomolecules. Other actuation methods requiring magnetic films, or conductive cantilevers also suffer from similar limitations.[12]

The actuation of AFM cantilevers using acoustic radiation pressure (ARP) was recently introduced.[13] This technique utilizes the acoustic radiation force generated by reflecting high-frequency (50–250 MHz) acoustic waves off

---

[a)]Author to whom correspondence should be addressed; electronic mail: ldegertekin@me.gatech.edu

the AFM cantilever. ARP actuation provides a broad bandwidth in the dc-MHz, enabling fast imaging and producing clean tuning curves. More importantly, it can be used with commercial AFM cantilevers with virtually any geometry and material. Tapping mode and elasticity imaging has been performed with an ARP actuation scheme, however, the ARP actuator geometry was not suitable for integration with conventional AFM imaging systems and therefore its use on a variety of samples was limited.[14]

In this article, we introduce a fluid cell for AFM with an integrated ARP actuator that can be used with a commercial AFM system. This fluid cell is capable of both dc and ac excitation of any cantilever without any spurious resonances. In the following, we first give a brief theory of operation of the ARP actuator. We then describe the ZnO thin film ARP transducer, details of the fluid-cell construction, and the custom-designed ARP driver electronics. Experimental characterization results obtained from the ARP actuator-integrated commercial AFM system are also presented. Finally, tapping mode imaging and molecular force spectroscopy results are presented and discussed as illustrative application examples.

II. THEORY OF OPERATION

The ARP actuator relies on the fact that a traveling acoustic wave carries a momentum, like an electromagnetic wave, which is partially reversed when it is reflected from a boundary. Such a momentum change dictates that the time average of pressure at the boundary cannot be zero and must be proportional to the magnitude of momentum change. Theoretical calculations of the radiation pressure were first made by Rayleigh, however, discussions about the correct calculation of the magnitude of the force continued for a long period of time.[15,16] Recent practical applications of ARP actuation include ultrasonic droplet ejection for ink printing and acoustovibrometry, where an amplitude-modulated ultrasound beam is used to remotely apply low-frequency forces to measure elastic properties of tissue as well as solid structures.[17,18]

For our purposes, one can consider the schematic shown in Fig. 1 to explain the principle of the ARP actuation of AFM cantilevers. An acoustic wave is reflected off the surface of a cantilever that has an overall pressure reflection coefficient of Γ. Note that for the focused beam case, a value of Γ can be computed as a weighted average of the reflection coefficients of plane waves with different directions. The time-averaged ARP force applied on the cantilever can be calculated by using the Langevin radiation pressure, Ω, given in Eq. (1), where I_i is the intensity of the incident acoustic wave and c is the speed of sound in the liquid medium,

$$\Omega = I_i \frac{2|\Gamma|^2}{c}. \tag{1}$$

This equation predicts 1.33 nN of force applied for 1 μW acoustic power for a perfectly reflecting boundary. But several loss mechanisms are in effect during the conversion of electrical power input to the ARP actuator transducer
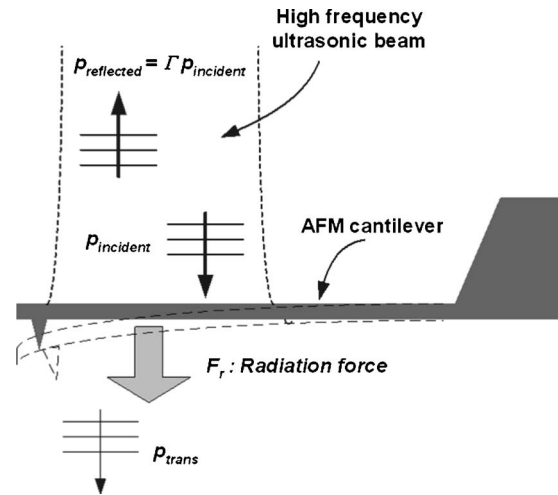

FIG. 1. Basic operation principle of acoustic radiation pressure actuator.

to acoustic power that reaches the cantilever. The sources of loss are piezoelectric material losses, impedance mismatch between the electrical generator and the transducer, acoustic attenuation in both transducer substrate and in liquid medium, and the inability of the unfocused transducer to project all available acoustic power on the relatively small area of most AFM cantilevers, i.e., diffraction losses.

Due to the quadratic dependence of the radiation force to the average value of instantaneous acoustic pressure, in order to apply a given amount of time-varying force, $F(t)$ (normalized to unity) to the cantilever, the rf input voltage needs to have a form given by $v(t) = C\sqrt{1+F(t)}\cos(\omega_c t)$, where ω_c denotes the carrier angular frequency in the rf range and C is a constant. The addition of 1 to $F(t)$ ensures that there will not be any clipping of the sinusoidal force applied to the cantilever, since the ARP actuator can only apply forces in a single direction. It should also be noted that the there is usually at least two orders of magnitude separation between the frequency of the applied force $F(t)$ and the carrier frequency.

III. INTEGRATION OF ARP ACTUATOR TO FLUID CELL

A. Fabrication of the fluid cell holder

The body of the custom fluid cell was designed in a three-dimensional (3D) modeling software and fabricated by high resolution stereolithography.[19] This process allowed the precision and complexity required in the final product as compared to conventional machining. The transducer chip, which has dimensions of 1.5 mm × 2.5 mm, is positioned at a 45° angle with respect to the sample surface, as illustrated in the schematic of Fig. 2. Since the cantilever to transducer distance is important for acoustic attenuation loss and streaming effects, this position was chosen as a compromise. The chip was located such that there is an imaginary line normal to the transducer surface that passes though the center of the piezoelectric transducer and intersects the cantilever very close to the tip location. This arrangement reduced the transducer to cantilever distance to approximately 1.45 mm while allowing optical access to the cantilever via an
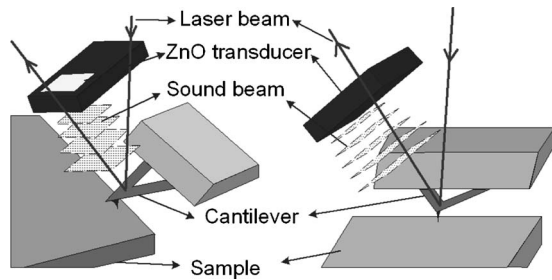
FIG. 2. Schematic of the practical implementation of the ARP actuator in a fluid cell with optical deflection detection.

FIG. 4. (a) Top view of the silicon chip with the ZnO transducer and its bond pads. (b) Silicon chip with three individual ZnO transducers with different sizes.

optical window made from polycarbonate. Since the positioning of the cantilever with respect to the transducer is important, custom alignment marks and recesses were built into the structure to aid positioning. A custom bracket, which mounts to the AFM head, was also designed in order to isolate the holder from external vibrations and forces that can come via the small diameter coaxial cable that carries the electrical signal to the transducer. A picture of the fluid cell is shown in Fig. 3, together with a close-up of the transducer and cantilever area.

B. ARP transducer

The piezoelectric acoustic transducer for the ARP actuator was fabricated on 330 μm thick 1.5 mm $\times$ 2.5 mm silicon substrate, and sputtered ZnO was used as the piezoelectric material [see Fig. 4(a)]. Fabrication involves a two-mask process, first one for the formation of the bottom electrode and second for the formation of an active ZnO element and the top electrode. The bottom electrode is evaporated Ti–Au film. The ZnO transducer element is deposited by direct magnetron sputtering and has an approximate thickness of 19 μm. The top electrode is also fabricated from gold. Both the 1.2 mm $\times$ 0.8 mm transducer element and the top electrode were defined by a single mask and formed by wet etching. Details of the fabrication process can be found elsewhere.[20] Note that arrays of ARP actuators can be formed easily using this fabrication process. As an example, an array of rectangular ZnO transducers of various sizes fabricated on a separate silicon substrate is shown in Fig. 4(b).

IV. CHARACTERIZATION OF THE ARP ACTUATOR

A. Electrical characterization

The electrical characteristics of the transducer were modeled with a standard one-dimensional KLM model that consists of an air-backed ZnO transducer on a silicon sub-

strate that is in contact with a fluid half-space, in this case made of water. The loss in ZnO thin film and the substrate material were modeled using finite quality factors of 40 and 240, respectively. Figure 5 shows the comparison between calculated and measured electrical impedance of the transducer operated in water. The individual sharp peaks, spaced approximately 13 MHz apart, are due to the cavity resonances inside the silicon substrate, which is the result of the large acoustic impedance mismatch between silicon and water. A much broader curve, which can be formed by the connecting the maxima of the peaks, represents the frequency response of the piezoelectric element radiating into a silicon half-space, as expected. In order to increase the efficiency thus to reduce the electrical impedance mismatch between the transducer and rf source at the desired operating frequency of 153 MHz, a simple serial inductor with a value of 0.68 μH was used, which resulted in an electrical reflection coefficient of $|\Gamma_e| = 0.4$.

B. Acoustic characterization

The acoustic actuation response of the actuator was measured by sweeping the carrier frequency while monitoring the AFM cantilever deflection. For this measurement, a V-shaped silicon nitride cantilever was driven at 1 kHz, below its resonant frequency, by modulating the carrier signal, as discussed earlier in this article. Note that using the lock-in amplifier instead of a rms detector allows the detection of only the first harmonic, removing the effect of the inherent
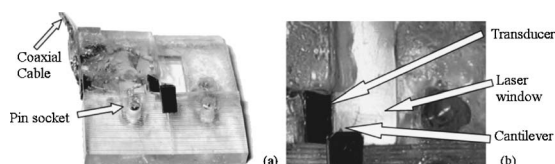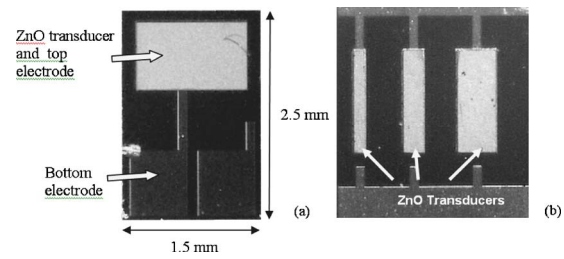

FIG. 3. (a) The fluid cell with an integrated ARP actuator. The main structure is made up of epoxy and shaped by laser stereolithography. (b) Close-up of the fluid cell showing the relative positions and orientation of the ARP actuator, AFM cantilever, and the optical window.
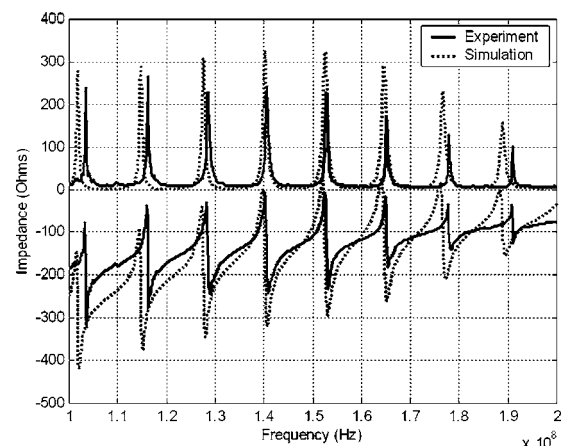

FIG. 5. Measured (solid line) and calculated (dotted line) electrical impedance of the ZnO transducer on a 0.33 mm thick silicon substrate. The transducer is designed for operation in the 120–150 MHz range.
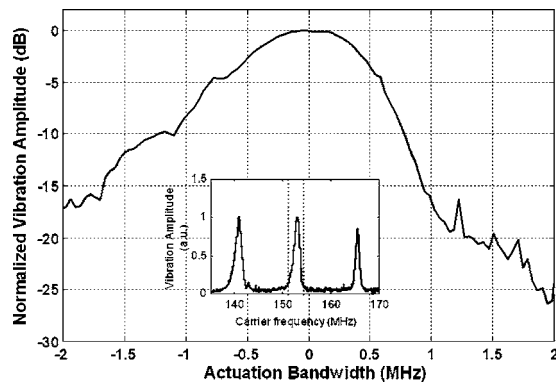
FIG. 6. Measured acoustic response of the ARP actuator around a carrier frequency of 153 MHz.
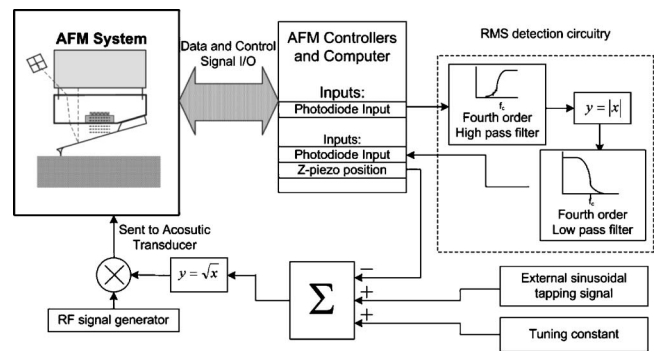

FIG. 7. The schematic of the electronics that integrates the ARP actuator to the commercial AFM controller for both vertical Z position control and ac excitation for tapping mode imaging.

nonlinearity of the ARP actuation method. The value of the observed cantilever vibration, around the selected 153 MHz peak of the device and normalized to its maximum value, is depicted in Fig. 6. The −3 dB bandwidth of the device around this peak is measured as 450 kHz. It should be noted that this peak is a direct result of the cavity resonance that forms inside the silicon transducer substrate and it is not an inherent characteristic of the piezoelectric element. It has been shown previously that ARP actuators with different substrates and matching layers can have bandwidths in the MHz range.[14]

Using a 140 μm long, 20 μm wide V-shaped silicon nitride cantilever with 0.1 N/m spring constant, we measured the losses in the ARP actuator system from the electrical input to the cantilever deflection. This observed value deflection is 78 dB less than the theoretical maximum value of 1.13 nN/μW mentioned in the first section of this article. The electrical impedance mismatch discussed earlier accounts for 1.5 dB of this loss. Acoustic attenuation in the water at 150 MHz contributes 14.6 dB of the loss according the tabulated values. Diffraction loss due to unfocused operation is 44 dB, and the less than unity pressure reflection from the cantilever surface and the reflections from the rigid sample surface pushing back the cantilever in the opposite direction contribute 10 dB. Finally, the 45° angle of the beam and the reflection coefficient of the cantilever, which was calculated as 0.4 for a 0.6 μm thick cantilever at 150 MHz, contribute 4.6 dB to the total loss. Overall, these simple considerations with plane wave approximations agree with the measured value to within a factor of 3. Note that cylindrical or spherical focusing can be used to reduce the diffraction losses by 20 dB, increasing the efficiency of the ARP actuator significantly, enabling its use for applications beyond the ones described here.[13]

V. ARP DRIVER ELECTRONICS

In order to use the ARP actuator for fast imaging, a number of changes to the existing commercial AFM system were made, as shown in Fig. 7.[21] The Z piezo in the AFM scanner head was deactivated by disconnecting it from the AFM controller. The low-voltage Z-piezo control signal from the AFM controller was then added to the ac tapping mode signal with appropriate coefficients. This signal represents the total amount of force to be applied on the cantilever. However, it needs to be modified by using a square root generator circuit before being used as the modulating signal for the rf generator, since the force applied by the ARP actuator is proportional to the power, not the amplitude, of the rf input signal, as discussed previously. The square root function is approximated by using a piecewise linear function, which is implemented by using an operational amplifier and a network of resistors that are progressively shorted by eight diodes.

Another limitation on system speed is the bandwidth of the rms detector that is used in a commercial AFM system, which is approximately 1.5 kHz.[22] A high-speed rms detector was constructed by cascading a high-pass filter, full wave rectifier, and a low-pass filter. Both the low- and high-pass filters are fourth-order Chebyshev-type filters implemented by using Tow–Thomas resonator circuits . The choice of Tow–Thomas resonator circuits enables the adjustment of the bandwidth of the rms detector simply by potentiometers. With this approach we were able to select different rms detector bandwidths for different cantilevers to optimize the scan speed. Usually 30%–35% of the fundamental resonant frequency of the cantilevers was selected as the cutoff frequency.

VI. APPLICATION EXAMPLES

A. Tapping mode imaging

For tapping mode imaging, a V-shaped silicon nitride cantilever ($k=0.1$ N/m) with a resonant frequency of 6.5 kHz in water was selected as a compromise between the speed and actuation range. The cantilever tip was located laterally around $10-15$ μm away from the edge of the sample surface to maximize the actuation range without the adverse effects of reflected waves from the sample. A free cantilever amplitude of 30 nm is used and the cantilever was excited at its resonant frequency. The cutoff frequency of the rms detector was set to 2 kHz due to the limitation imposed by the low resonant frequency of the cantilever. Figure 8 shows the oscillation amplitude versus. vertical position curve, i.e., the approach curve, which was acquired using conventional Z piezo of the AFM system. The approach curve is free of actuation artifacts and it has a near-unity slope after the cantilever starts intermittent contact with the
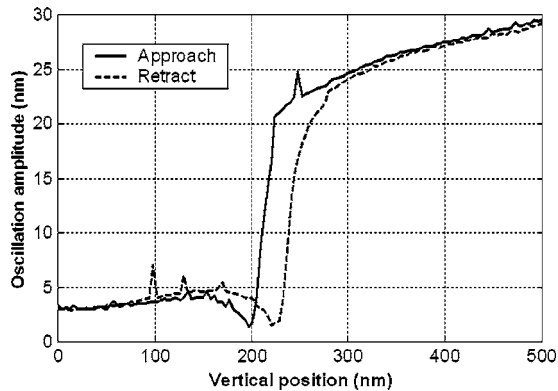
FIG. 8. Measured tapping mode approach and retract curves for an ARP-actuated cantilever at 6.5 kHz.

surface. Note that the Z piezo of the commercial AFM was used to extend the vertical range of the approach curve measurement to clearly illustrate the actuator characteristics.

For a demonstration of the tapping mode imaging capability using the ARP actuator as the only actuator, the same cantilever of Fig. 8 was used. With the Z piezo disconnected and 26 dBm electrical power input to the ZnO transducer, the ARP actuator had a 130 nm dc actuation range, which is adequate for the imaging of most biomolecular samples. During imaging, the PID feedback controller of the commercial AFM system was used with no proportional gain and the integral gain was experimentally adjusted close to the stability limit. The imaging results obtained on a sample with 2.5 μm wide, 30 nm thick aluminum fingers deposited on a polished silicon substrate. Figure 10, later, shows the image acquired with all acoustic ARP actuation [Fig. 9(a)] as well

as an image of the same region acquired with regular contact mode operation [Fig. 9(b)]. A comparison of the cross sections of two images is shown in Fig. 9(c). The good agreement between the traces and low noise level in the images should be noted.

B. Force spectroscopy measurements on single molecules

To test the capability of the ARP actuator for conducting single molecular experiments, we measured unbinding forces between $\alpha_5\beta_1$ integrin (reconstituted in the coverglass-supported lipid bilayer) and fibrinectin (adsorbed on the cantilever tip). Binding was infrequent, ensuring dominant single molecular interactions, yet much higher than that between the same $\alpha_5\beta_1$ bilayer and a control cantilever tip coated with a noninteracting molecule (BSA), ensuring binding specificity. The cantilever tip was first brought to within 0.4 μm of the $\alpha_5\beta_1$ bilayer by a PZT actuator. Then the PZT actuator was disabled and the ARP actuator was turned on to drive the cantilever in repeated approach–contact–retraction cycles. Two such cycles with separate approach and retraction sections are exemplified in Fig. 10. Here, the tip deflection was monitored by a photodetector and converted to force (ordinate) using the spring constant of the AFM cantilever, which is plotted against the ARP driving force (bottom abscissas) and time (top abscissas, only the retraction phase). It is evident that single [Fig. 10(b)] unbinding events were clearly observed, demonstrating the feasibility of ARP-driven AFM for single molecule measurements to generate statistically significant data. The deviations of the approach curve from a flat line are due to the calibration procedure
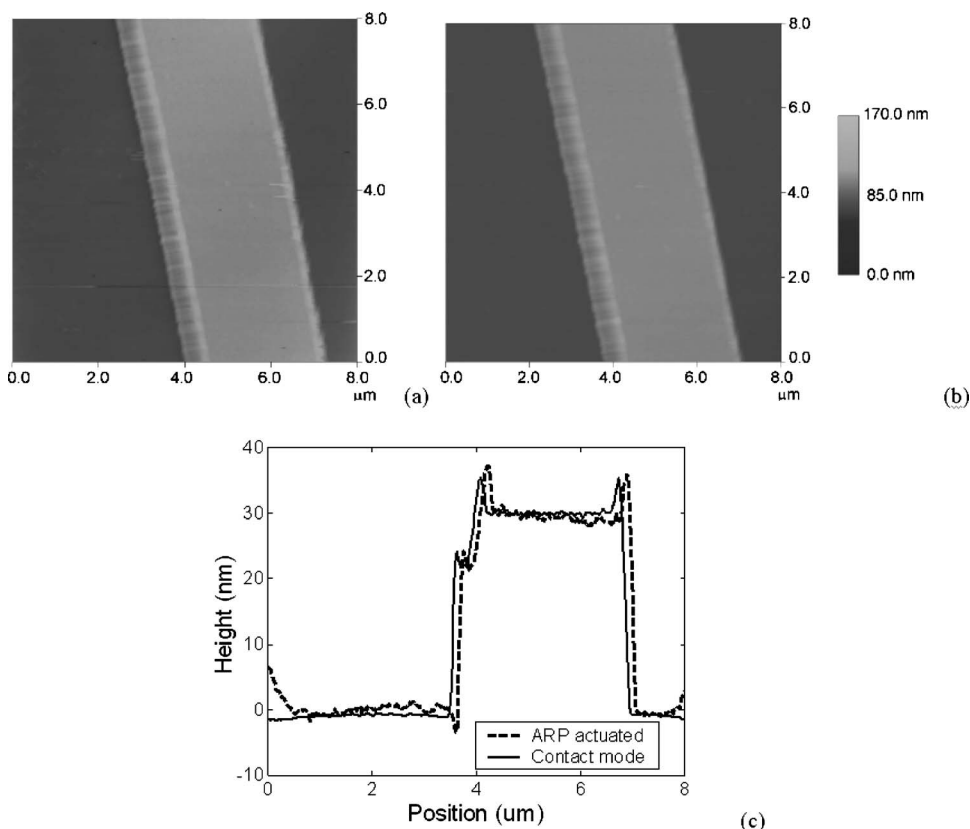

FIG. 9. (a) Tapping mode image of a 40 nm thick aluminum line on silicon acquired in water using the ARP actuator for both vertical Z positioning and ac excitation. (b) Contact mode image of the same sample. (c) Typical line scans from the tapping mode and contact images.
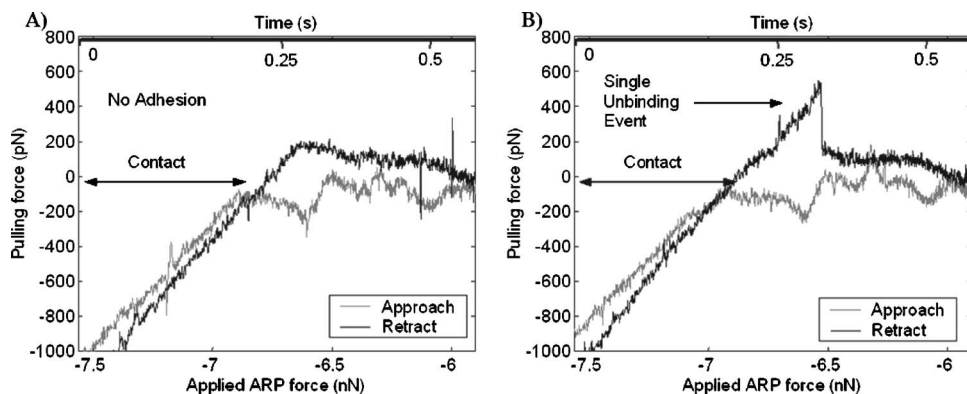
FIG. 10. The approach and retract curves for the ARP-driven AFM cantilever curves corresponding to (a) no adhesion; (b) single unbinding event.

used. Nevertheless, the repeatability of the curves is impressive for these initial measurements. The rms noise in the measurements is ~30 pN, which is mainly due to the mechanical vibration of the commercial AFM system. With better vibration isolation, this figure will be significantly improved.

VII. CONCLUSION

The ARP actuator is integrated to a fluid cell compatible with a commercial AFM system to perform most standard imaging and force spectroscopy measurements, as demonstrated with the results presented. With its flexibility to drive any type of cantilever and broad bandwidth including dc actuation capability makes it suitable, especially for demanding high-speed imaging applications. The ARP actuator is fabricated using well-known ZnO deposition and microfabrication techniques, which can be used to form arrays of focused actuators with higher efficiency and capability of actuating individual cantilevers in 1D or 2D arrays. In our current work we aim to initially develop 1D actuator arrays for parallel single molecular force spectroscopy and then apply the technique for fast, parallel imaging in fluids.

ACKNOWLEDGMENTS

[1] P. K. Hansma et al., Appl. Phys. Lett. **64**, 1738 (1994).
[2] M. A. Poggi, E. D. Gadsby, L. A. Bottomley, W. P. King, E. Oroudjev, and H. Hansma, Anal. Chem. **76**, 3429 (2004).
[3] T. E. Schaffer, J. P. Cleveland, F. Ohnesorge, D. A. Walters, and P. K. Hansma, J. Appl. Phys. **80**, 3622 (1996).
[4] M. B. Viani et al., Rev. Sci. Instrum. **70**, 4300 (1999).
[5] B. T. Marshall, K. K. Sarangapani, J. H. Lou, R. P. McEver, and C. Zhu, Biophys. J. **88**, 1458 (2005).
[6] M. B. Viani, T. E. Schaffer, A. Chand, M. Rief, H. E. Gaub, and P. K. Hansma, J. Appl. Phys. **86**, 2258 (1999).
[7] S. C. Minne, G. Yaralioglu, S. R. Manalis, J. D. Adams, J. Zesch, A. Atalar, and C. F. Quate, Appl. Phys. Lett. **72**, 2340 (1998).
[8] T. Ando, N. Kodera, E. Takai, D. Maruyama, K. Saito, and A. Toda, Proc. Natl. Acad. Sci. U.S.A. **98**, 12468 (2001).
[9] T. Sulchek, S. C. Minne, J. D. Adams, D. A. Fletcher, A. Atalar, C. F. Quate, and D. M. Adderton, Appl. Phys. Lett. **75**, 1637 (1999).
[10] T. Sulchek, R. Hsieh, J. D. Adams, G. G. Yaralioglu, S. C. Minne, C. F. Quate, J. P. Cleveland, A. Atalar, and D. M. Adderton, Appl. Phys. Lett. **76**, 1473 (2000).
[11] B. Rogers et al., Rev. Sci. Instrum. **74**, 4683 (2003).
[12] W. H. Han, S. M. Lindsay, and T. W. Jing, Appl. Phys. Lett. **69**, 4111 (1996).
[13] F. L. Degertekin, B. Hadimioglu, T. Sulchek, and C. F. Quate, Appl. Phys. Lett. **78**, 1628 (2001).
[14] A. G. Onaran, F. L. Degertekin, and B. Hadimioglu, Appl. Phys. Lett. **80**, 4063 (2002).
[15] R. T. Beyer, J. Acoust. Soc. Am. **63**, 1025 (1978).
[16] B. T. Chu and R. E. Apfel, J. Acoust. Soc. Am. **72**, 1673 (1982).
[17] M. Fatemi and J. F. Greenleaf, Science **280**, 82 (1998).
[18] S. A. Elrod, A. B. Hadimioglu, B. T. Khuriyakub, E. G. Rawson, E. Richley, C. F. Quate, N. N. Mansour, and T. S. Lundgren, J. Appl. Phys. **65**, 3441 (1989).
[19] Viper si2 SLA System, 3D Systems, Valencia, CA.
[20] S. R. Manalis, S. C. Minne, and C. F. Quate, Appl. Phys. Lett. **68**, 871 (1996).
[21] Nanoscope 3100, Digital Instruments, Santa Barbara, CA.
[22] T. Sulchek, G. G. Yaralioglu, C. F. Quate, and S. C. Minne, Rev. Sci. Instrum. **73**, 2928 (2002).